

# An Optimization Method for Quantifying Magnetization Vectors in Magnetic Resonance Measurements

Leila Borvayeh<sup>\*1</sup>, Mohammad Sabati<sup>2</sup>, Raouf Mbarki<sup>3</sup>

<sup>\*1</sup>Department of Mathematics, Australian College of Kuwait, West Mishref, Kuwait

<sup>2</sup>Department of Electrical Engineering, Australian College of Kuwait, West Mishref, Kuwait

<sup>3</sup>Department of Mechanical Engineering, Australian College of Kuwait, West Mishref, Kuwait

## ABSTRACT

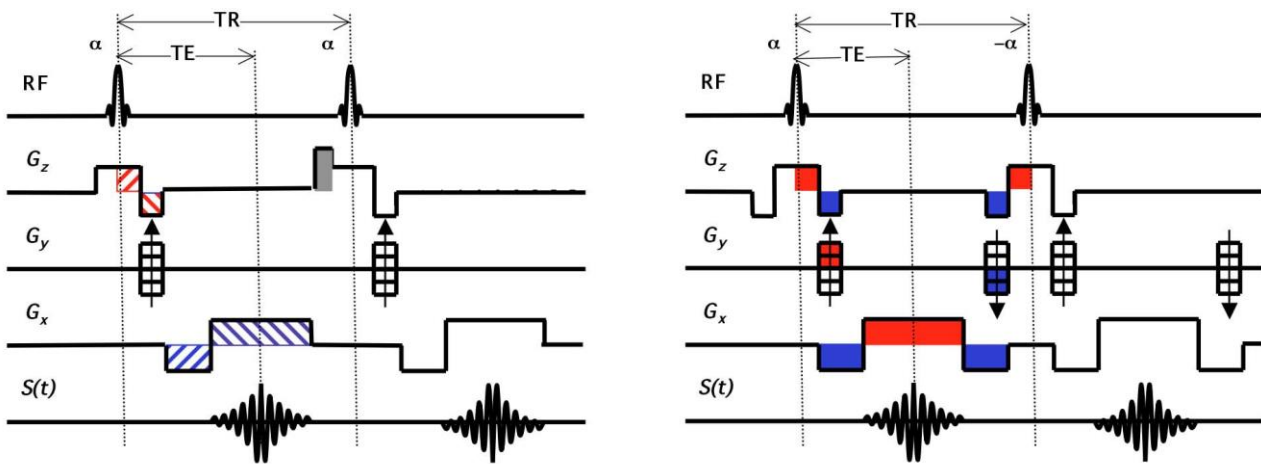
There are increasing interests in quantitative magnetic resonance (MR) measurement techniques for a variety of experimental physics and clinical applications. Recently methods for quantification of local nuclei magnetization magnitude,  $M_0$ , and its longitudinal relaxation time ( $T_1$ ) have been proposed. An efficient method for measuring  $T_1$  values is based on acquiring two spoiled gradient-recalled echo (SPGR) data sets in steady states with different radiofrequency (RF) excitation flip angles, which has also been extended, with additional acquisitions, to obtain  $M_0$  values representing the object's proton density. Several factors, including inaccurate flip angles due to inhomogeneity of the exciting RF magnetic fields and low signal-to-noise ratios (SNR) may negatively affect the accuracy of this method and produce systematic errors in the  $T_1$  and  $M_0$  estimations. In this paper, a modified dual-acquisition method based on an optimization of the SPGR MR sequence formulism is presented for reliable  $M_0$  and its actual flip angle (i.e., magnetization vector,  $M$ ) measurements with a high spatial resolution and a relatively short experimental time. The optimal nominal flip angles for  $M_0$  measurements and the optimal repetition times for estimation of the RF excitation angles are found analytically and numerically using the SPGR MR sequence. The proposed method can measure the magnetization vectors with an isotropic spatial resolution of  $1 \times 1 \times 1 \text{ mm}^3$  of a large 3D object in less than 5 minutes.

**Keywords:** Optimization, Magnetic Resonance (MR), Nuclei Magnetization Vector, Quantitative Analysis, MR Data Acquisition, Longitudinal Relaxation Time, Flip Angle.

## I. INTRODUCTION

Magnetic resonance (MR) technique is now a routine modality for clinical imaging and it is also used for experimental physics studies of various applications including spectroscopy and non-destructive characterization of soft materials. It is considered a minimally invasive approach in that harmful ionizing x-ray radiation is not used and its adverse reactions are negligible. Technically, however, in MR, the scan time, the signal-to-noise ratio (SNR), and the spatial

and temporal resolutions are inherently interdependent. The fixed relationship between these properties causes trade-offs that improving one characteristic would worsen the others. Steady-state free precession (SSFP) MR pulse sequence techniques were first introduced in 1958 (1) and later re-introduced in 1986 (2).



(a) SPGR

(b) bSSFP

**Figure 1.** Pulse sequence timing diagrams comparing (a) spoiled gradient-recalled echo (SPGR) and (b) balanced steady-state free precession (bSSFP). Both sequences generate an MR signal using a combination of radio frequency (RF) excitation and spatial gradient ( $G_x$ ,  $G_y$ , and  $G_z$ ) pulses. The main difference is that bSSFP is fully balanced whereby the magnetization is fully refocused prior to each excitation – over each TR interval the red and blue gradients sum to zero. By comparison, in SPGR, gradients are arranged to ensure echo formation at the echo time (TE), but unequal areas and the added grey gradients destroy (dephase) any remaining transverse magnetization before the next excitation. The refocusing of the magnetization in bSSFP increases signal-to-noise ratio (SNR) but at the expense of having a higher sensitivity to off-resonance effects.

Re-introduction was a result of these sequences being technically challenging and placing tremendous demands on the MR instrument software and hardware. SSFP sequences can be broadly classified as either incoherent (e.g., spoiled gradient-recalled echo, SPGR) or coherent (e.g., balanced SSFP). The main difference between the methods lies in whether the transverse magnetization is spoiled (i.e., destroyed due to unbalanced gradients, Fig 1a) or refocused (due to balanced gradients, Fig 1b) between successive RF excitation pulses. Owing to their use of small flip angles and intentional destruction (or spoiling) of the transverse magnetization, the inherent contrast between soft tissues, such as blood and muscle, is dominated by  $T_1$  and to a lesser extent  $T_2^*$ . By comparison, bSSFP techniques refocus the magnetization (Fig 1b), resulting in high SNR but image contrast is proportional to the ratio of  $T_2/T_1$  (3). Unlike SPGR, bSSFP sequences, in practice, suffer from the banding artifacts, due to the requirement of highly balanced gradient fields, dependency to both  $T_1$  and  $T_2$  values, and the time needed for the magnetization to reach

the steady state to avoid image artifacts and the high signal from surrounding tissue like the body fat (4,5). Reaching steady state can take up to  $5 \times T_1$  (typically 1 s to 6 s) depending on the object content and imaging parameters, during which the MR signal fluctuates; acquisition in the non-steady-state can cause image artifacts, such as ghosting and blurring (4-6). For these reasons, the SPGR sequences have been the base for recent methods for quantitative measurements of the tissue  $T_1$  and magnetization magnitude,  $M_0$  (7-12). The acquisition of two SPGR data sets with different flip angles has allowed for the calculation of  $T_1$  and  $M_0$  maps with a high spatial resolution and a relatively short experimental duration.

In this study, we present a modified two-acquisition SPGR methods for the measurement of the MR magnetization vector. Linear parameterization is used to independently estimate the actual flip angle and the magnitude of the magnetization throughout the object. First, we analytically derive the optimal flip angles for SNR-optimized  $M_0$  magnitude maps and verify the results in normal subjects on an MR

instrument. Then, we analytically and numerically derive optimal repetition times for SNR-optimized flip angle inhomogeneity maps. It is demonstrated that accurate and reliable magnetization maps can be obtained with an isotropic resolution of 1 mm that covers the entire a large volumetric object as size of a human brain in an acceptable scan time using only two acquisitions.

## II. METHODS AND MATERIAL

### M<sub>0</sub> Mapping Using Variable Flip Angles

Figure 2 represent the magnetization vector, **M**, in a typical MR experiment in the presence of the external magnetic field **B**<sub>0</sub> and RF transmit/receive coil.

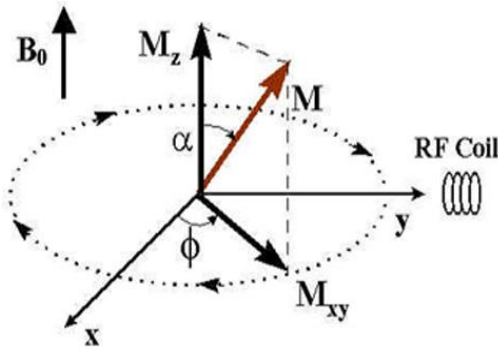


**Figure 2.** Magnetization vector, **M**, in a typical MR experiment. In the presence of an external magnetic field **B**<sub>0</sub>, the RF coil is used for exciting the **M** (tipping it out of equilibrium) and for detecting the transverse component of **M**, **M**<sub>xy</sub>.

The variable flip angle SPGR approach for **M**<sub>0</sub> mapping is based on the dependence of the steady-state signal of the SPGR sequence with the nominal flip angle  $\alpha$ , the repetition time **TR**, the echo time **TE**, and a factor that is proportional to the proton density and the equilibrium longitudinal magnetization **M**<sub>0</sub>:

$$S = M_0 \cdot \frac{1 - \exp(-TR/T_1)}{1 - \cos(B_1\alpha) \cdot \exp(-TR/T_1) \cdot \sin(B_1\alpha) \cdot \exp(-TE/T_2^*)} \quad [1]$$

where **M**<sub>0</sub> is the equilibrium magnetization directly proportional to the voxel water content, **B**<sub>1</sub> is the actual-to-nominal flip angle ratio (ideally equals to

1.0). **M**<sub>0</sub> is the signal that would be obtained with  $\alpha = 90^\circ$ , **B**<sub>1</sub> = 1.0, **TR** » **T**<sub>1</sub>, and **TE** « **T**<sub>2</sub><sup>\*</sup>. SNR calculation and optimization of flip angles have been previously studied for **T**<sub>1</sub> mapping (7,8). Here, we focus on the determination of these parameters for **M**<sub>0</sub> mapping. Without loss of generality, **B**<sub>1</sub> = 1.0 is assumed for the following calculations and its effect is then applied at later steps.

Defining  $E = \exp(-TR/T_1)$  and  $E^* = \exp(-TE/T_2^*)$ , adapted from Deoni et al [7] this equation can be linearized:

$$\frac{S}{\sin(\alpha)} = M_0(1 - E)E^* + \frac{S}{\tan(\alpha)}E \quad [2]$$

Thus, a plot of  $S/\sin(\alpha)$  versus  $S/\tan(\alpha)$  yields a straight line of  $Y = b + X \cdot m$ , allowing **M**<sub>0</sub>**E**<sup>\*</sup> and **T**<sub>1</sub> to be determined from the slope **m** and the constant **b** as follow:

$$T_1 = -\frac{TR}{\ln(m)} \quad \text{and} \quad M_0E^* = \frac{b}{1-m} \quad [3][3]$$

If only two acquisitions with different flip angles  $\alpha_1$  and  $\alpha_2$  (i.e., **S**<sub>1</sub> and **S**<sub>2</sub>) are performed, **M**<sub>0</sub>**E**<sup>\*</sup> can be calculated from:

$$M_0E^* = \frac{AS_1S_2}{BS_2 - CS_1} \quad [4]$$

where:

$$A = \sin(\alpha_2) \tan(\alpha_1) - \sin(\alpha_1) \tan(\alpha_2)$$

$$B = \tan(\alpha_1) \sin(\alpha_1) (\sin(\alpha_2) - \tan(\alpha_2)) \quad [5]$$

$$C = \tan(\alpha_2) \sin(\alpha_2) (\sin(\alpha_1) - \tan(\alpha_1)).$$

**T**<sub>1</sub> values can also be determined using a similar method that has been previously studied and optimized by others [c.f. Refs. (7,8,13)]. Provided the two measurements with  $\alpha_1$  and  $\alpha_2$  (i.e., **S**<sub>1</sub> and **S**<sub>2</sub>, respectively) are performed with the same bandwidth (**BW**) and receiver gain, the noise level  $\sigma_s$  is the same

in both measurements. The noise in the  $M_0$  map is then given by:

$$\sigma_{M_0} = \sqrt{\left(\frac{\partial M_0}{\partial S_1}\right)^2 + \left(\frac{\partial M_0}{\partial S_2}\right)^2} \sigma_s \quad [6]$$

The partial derivatives can be calculated from Eq. [4]:

$$E^* \frac{\partial M_0}{\partial S_1} = \frac{ABS_2^2}{(BS_2-CS_1)^2} \quad \text{and} \quad E^* \frac{\partial M_0}{\partial S_2} = \frac{-ACS_1^2}{(BS_2-CS_1)^2} \quad [7]$$

A combination of Eqs. [6] and [7] yields:

$$\sigma_{M_0} = \frac{A}{E^*} \sqrt{\frac{B^2 S_2^4 + C^2 S_1^4}{(BS_2-CS_1)^2}} \cdot \sigma_s \quad [8]$$

Thus, in order to maximize the SNR in the  $M_0$  map, the pair of flip angles  $(\alpha_1, \alpha_2)$  which minimizes this expression has to be found numerically.

### $B_1$ Mapping Using Variable Repetition Times

Using a similar approach for  $M_0$  estimation (11,13), the variable repetition time SPGR approach for  $B_1$  mapping is based on the dependence of the steady-state signal on the flip angle  $\alpha$ , the repetition time TR, the echo time TE, and the  $M_0$  (see Eq. [1]). Defining  $E = \exp(-TR/T_1)$  and  $E^* = \exp(-TE/T_2^*)$ , as above, this equation can now be linearized as:

$$\frac{1-E}{S} = \frac{1}{S_0 E^* \tan(B_1 \alpha)} (-E) + \frac{1}{S_0 E^* \sin(B_1 \alpha)} \quad [2][9]$$

Thus, a plot of  $(1-E)/S$  versus  $-E$  yields a straight line of  $Y = m.X + b$  and  $B_1$  can be determined from the ratio of the slope  $m$  and the constant  $b$ . If only two acquisitions with different repetition times  $TR_1$  and  $TR_2$  (i.e.,  $E_1$  and  $E_2$ ) are performed,  $B_1$  can be calculated from:

$$B_1 = \frac{1}{\alpha} \cos^{-1} \left( \frac{m}{b} \right) \quad [3a] \quad [10a]$$

with

$$m = SL = \frac{S_2 - S_1 + E_2 S_1 - E_1 S_2}{S_2 S_1 (E_2 - E_1)} \quad [3b][10b]$$

and

$$b = \text{const.} = \frac{E_2 S_2 (1 - E_1) - E_1 S_1 (1 - E_2)}{S_2 S_1 (E_2 - E_1)} \quad [3c] \quad [10c]$$

and

$$SR = \frac{m}{b} = \frac{S_2 - S_1 + E_2 S_1 - E_1 S_2}{E_2 S_2 (1 - E_1) - E_1 S_1 (1 - E_2)} \quad [3d] \quad [10d]$$

Provided the two measurements with  $TR_1$  and  $TR_2$  (i.e.,  $E_1$  and  $E_2$ , respectively) are performed with the same bandwidth (BW) and receiver gain, the noise level  $\sigma_s$  is the same in both images. The noise in the  $B_1$  map is then given by:

$$\sigma_{B_1} = \sqrt{\left(\frac{\partial B_1}{\partial S_1}\right)^2 + \left(\frac{\partial B_1}{\partial S_2}\right)^2} \sigma_s \quad [4] \quad [11]$$

The partial derivatives can be calculated from Eq. [3a]:

$$\frac{\partial B_1}{\partial S_k} = \frac{1}{\alpha} \cdot \frac{-1}{\sin(B_1 \alpha)} \cdot \frac{\partial (SR)}{\partial S_k} \quad [5] \quad [12]$$

Using the expression for SR given in Eq. [10b] yields:

$$\frac{\partial (SR)}{\partial S_1} = \frac{S_2 (1 - E_1) (1 - E_2) (E_1 - E_2)}{[E_2 S_2 (1 - E_1) - E_1 S_1 (1 - E_2)]^2} \quad [6] \quad [13]$$

Due to the symmetry of Eq. [10d], a similar expression can be obtained for the partial derivative with respect to  $S_2$  by swapping the indices in Eq. [13]. A combination of Eqs. [11],[12], and [13] yields:

$$\sigma_{B_1} = \frac{-1}{\alpha \sin(B_1 \alpha)} \cdot \frac{(1 - E_1) (1 - E_2) |E_2 - E_1| \sqrt{S_1^2 + S_2^2}}{[E_2 S_2 (1 - E_1) - E_1 S_1 (1 - E_2)]^2} \cdot \sigma_s \quad [7] \quad [14]$$

Thus, in order to maximize the SNR in the  $B_1$  map, the pair of repetition times  $(TR_1, TR_2)$  which minimizes this expression has to be found numerically. Although the exact localization of the

minimum  $\sigma_{B_1}$  depends on  $B_1$ , the minima are quite broad and the range of  $B_1$  values of inside the human brain is sufficiently small and varies smoothly. Thus, the optimum repetition times for the different flip angles used in this work were determined for an intermediate, nominal  $B_1$  of 1.0.

**Optimum Repetition Times: Numerical Solution**

To determine which two repetition times to use for a particular  $(\alpha, T_1)$  combination in a more straightforward manner, consider the estimation of  $B_1$  from the linearized signal. The two signal intensities provide two points on the regression line. If each point suffers the same uncertainty, the further the two points are separated along the line, the better the estimate of slope. This separation along the ordinate can be defined as the normalized dynamic range (DR) of the regression line, given by:

$$DR = \frac{1-E_1}{S_1} - \frac{1-E_2}{S_2} \quad [15]$$

In our case, the data points do not suffer the same uncertainty; rather, the precision depends on the location of the points along the line and generally decreases as the two points move away from the midpoint (defined by the location of the peak of the signal curve and given by the Ernst signal ( $S_E$ )). This means that the precision can be related to the fractional signal of the points (FS).

$$FS = \frac{S_1 - S_2}{2S_E} \quad [16]$$

With the above considerations of the trade-off between DR and FS, we propose that optimum  $B_1$  precision will be achieved when the product of  $DR \times FS$  is maximized.

For the experimental evaluations, variable-flip angle SPGR scans with the following parameters were used on data obtained from two volunteers: TR/TE = 8.5/3.6 ms, flip angles: 3° and 17° (optimal flip angles for  $M_0$  mapping, see theory section and Fig 3), acquisition matrix = 256 × 256, receiver bandwidth = 210 Hz/Px, FOV = 256 mm × 256 mm, 135 slices, 1-

mm slice thickness, no gap between slices, parallel-imaging acceleration factor of 2 with 24 auto-calibration lines, and total acquisition time of 2 min and 28 seconds per each SPGR scan.

**III. RESULTS**

To maximize the SNR in the  $M_0$  magnitude map, the pair of flip angles ( $\alpha_1, \alpha_2$ ) that minimizes Eq. [6] for a given TR value can be found numerically as shown in Fig 3. Although the exact localization of the minimum depends on  $T_1$  (via  $S_1$  and  $S_2$ ), the minima are broad and the range of  $T_1$  values. Note, however, that the nominal  $M_0$  magnitude map is calculated directly from the measured SPGR signals  $S_1$  and  $S_2$ , and the flip angles only (see Eq. [4]), independent of  $T_1$  calculations. For short TR's, a small flip angle ( $< 5^\circ$ ) is favorably yielded, for which  $\sin(\alpha)$  can be approximated with  $\alpha$  so that the related SPGR image can be used for  $B_1$  estimate after appropriate processing (9, 11).

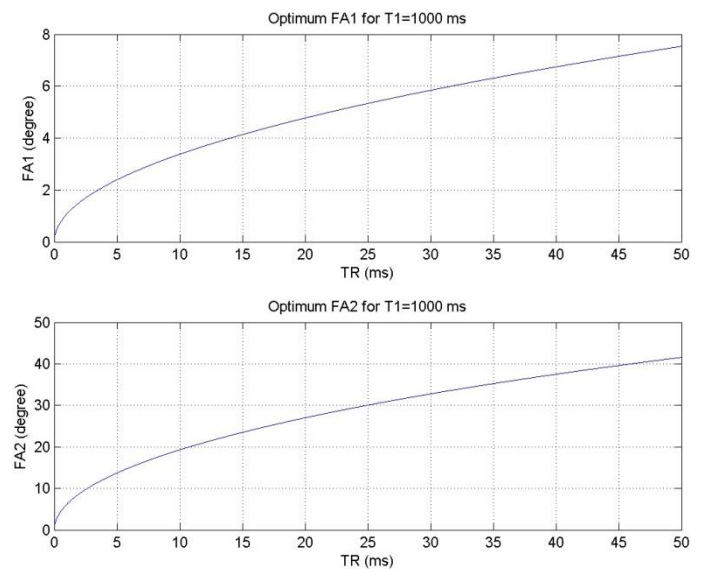
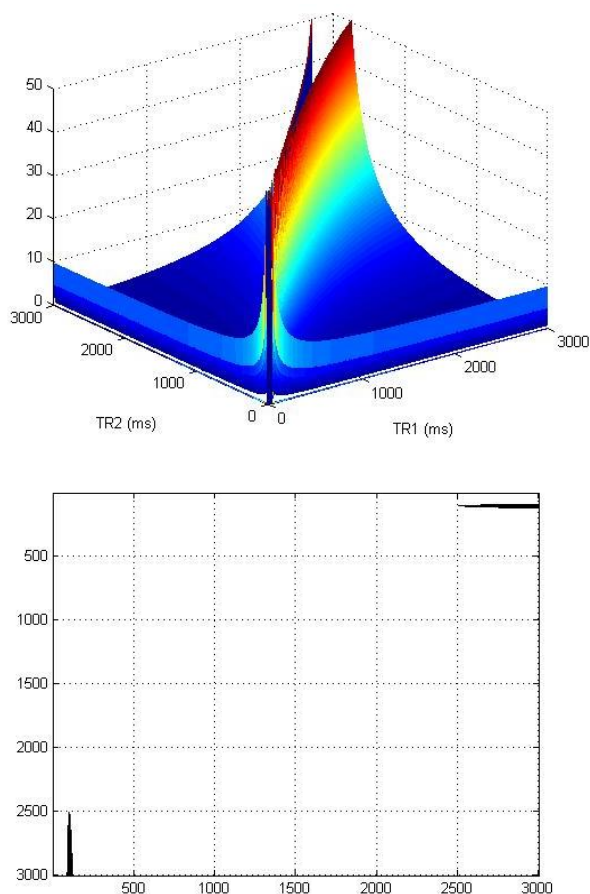


**Figure 3.** Optimal flip angles as a function of TR to obtain maximum-SNR for  $M_0$  mapping using dual SPGR-acquisitions obtained by numerical solution of Eq. [6].  $T_1=1000$  ms was assumed. TR=8.5 ms was used.

Figure 4 shows the  $\sigma_{B_1}$  as a function of TR's to obtain maximum SNR as per Eq. [14] for  $B_1$  mapping using the dual SPGR-acquisition obtained by numerical

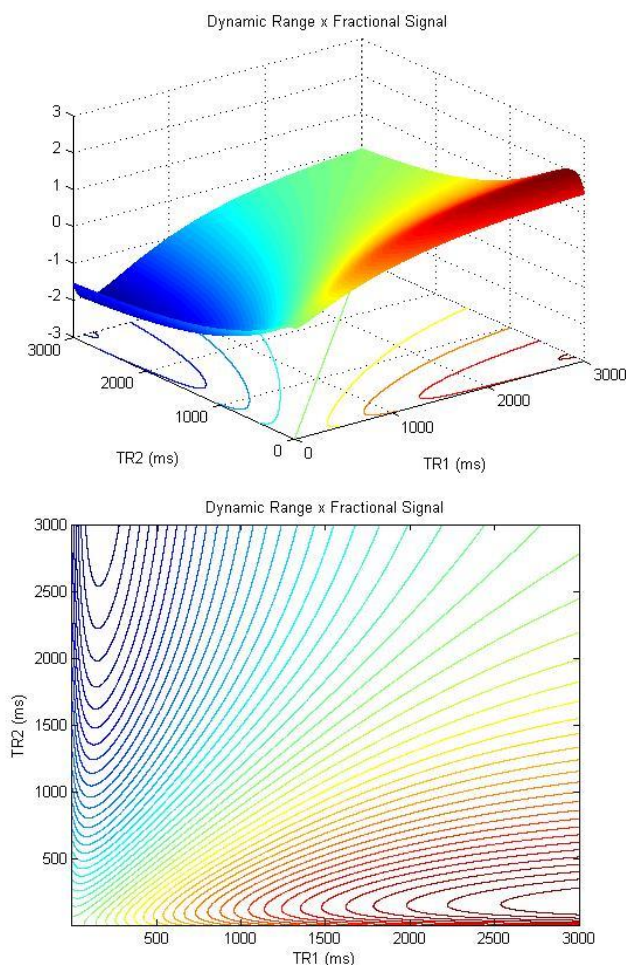
solution.  $T_1 = 1000$  ms was assumed. Although the exact localization of the minimum  $\sigma_{B_1}$  depends on  $B_1$ , the minima are quite broad and the range of  $B_1$  values, for example in the human brain is sufficiently small and varies smoothly. Thus, the optimum repetition times for the different flip angles used in this work were determined for an intermediate, nominal  $B_1$  of 1.0.

Figure 5 is a resultant plot of  $DR \times FS$ , from which the ideal repetition times can be determined. In this example, where we have used the same values as above, we confirm the prediction of the above ideal TR's as  $\sim 180$  ms and  $\gg T_1$  (in practice, any  $TR > 3$ s is sufficient). Due to the strong agreement between our analytical and intuitive results, we believe the  $DR \times FS$  product can be used to determine the repetition times for any  $(\alpha, T_1)$  case.



**Figure 4.** Optimal repetition times (TR's) as a function of TR (top: 3D plot of noise level; bottom: contour at the minimum noise level) to obtain maximum-SNR for  $B_1$  mapping using dual SPGR-acquisition obtained

by numerical solution of Eq. [14].  $T_1 = 1000$  ms was assumed. Optimum values of TR's  $\sim 180$  ms and  $\gg T_1$  were found.



**Figure 5.** A plot of  $DR \times FS$ , from which the ideal TR's can be determined (top: 3D plot of  $DR \times FS$ ; bottom: contour at the minimum  $DR \times FS$ ). Same values as with the analytical solutions (refer to the text) were used obtaining the same optimum values of the TR's of  $\sim 180$  ms and  $\gg T_1$  (in practice,  $TR > 3$  s) and confirming strong agreement with the analytical results.

Figure 6 illustrates a representative estimated 3D transmit/receive  $B_1$  map in three orthogonal planes obtained from the small-flip angle SPGR image. The grey-scale map represents a wide  $B_1$  range of 0.62–1.35 in the whole brain.

## IV. DISCUSSION

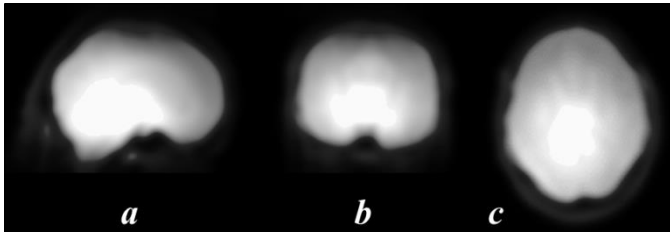


**Figure 6.** Representative of 3D combined transmit/receive  $B_1$  map (a: sagittal; b: coronal; c: axial) estimated by smoothing of the original SPGR images acquired with small flip angle ( $\alpha = 3^\circ$ ) that are linearly affected by the nonuniformity of the radio frequency  $B_1$  profile and normalized to 1.0. grey-scale range: 0.62–1.35 within the brain.

Figure 7 shows the estimated quantitative  $B_1$  (from the low-angle acquired SPGR image),  $B_1$ -imposed magnetization map, and the  $B_1$ -removed  $M_0$  magnitude maps at a middle slice obtained from a healthy volunteer. Notice the high  $B_1$  nonuniformity effects in the magnetization vector. The  $B_1$  map were properly estimated and removed so that correct  $M_0$  magnitude map were obtained throughout the brain.

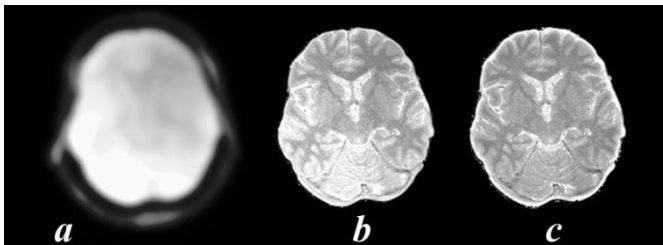


**Figure 7.** Representative 1-mm isotropic resolution slices of the estimated  $B_1$ , the  $B_1$ -imposed magnetization vector  $\mathbf{M}$ , and water content  $M_0$  maps from a healthy subject obtained by using the ( $3^\circ$ ,  $17^\circ$ )-flip angle pair. Excellent-quality maps were obtained.  $B_1$ -imposed magnetization map with clear  $B_1$ -nonuniformity evident is also shown for comparison.  $M_0$  values were normalized to cerebral spinal fluid (CSF)  $M_0$  values, assuming 100% water concentration (see text).

Accurate mapping of magnetization vector with high spatial resolution and short data acquisition times is technically challenging (14,15), particularly for in vivo measurements. In this study, we demonstrated that the dual-acquisition methods can be optimized for  $M_0$  mapping of a 3D object. The method presented in this study can correct for RF field effects by finding optimal excitation angles, appropriate acquisition parameters, a good  $B_1$  map estimate, and by using a reference of 100% water concentration (16,17). Due to its volumetric and high SNR, and post-processed  $B_1$  estimation, the proposed method can provide fast, efficient, and high-quality maps of the tissue water content. Additional acquisitions can be used to obtain  $B_1$  independently (see Figs. 4 and 5) in the expense of extra scan time.

The  $M_0$  mapping approach proposed by others (10, 15), based on five acquisitions, produced acceptable water measurement for a single voxel at 1.5 Tesla. However, the concomitant increase in scan time and the examination preparations render the technique intractable in a practical in vivo environment and also more susceptible to subject motion.  $M_0$  mapping on the basis of the variable flip angle approach yields reproducible results, potentially making it suitable for use in water-content experimental studies. This view is also supported by a recent study by Volz et al (18), that reported reliable and robust  $M_0$  mapping results after correcting of systematic errors. It is expected that this will be also true for the variable flip angle  $M_0$  mapping approach as the  $M_0$  values obtained in this study are comparable to those obtained with more sophisticated, multi-acquisition methods (15,19).

Further studies are required to verify the pathologic detectability of the proposed  $M_0$  mapping method in patients with local and global mild to moderate tissue water changes and to evaluate the clinical usefulness of  $M_0$  map in the neurological disorders. It should be noted that  $B_1$  estimate based on smoothing of the small-flip angle SPGR image may no longer be

accurate in cases of pathology where severe hypo or hyper intense regions may present. In such cases, the proposed  $B_1$  mapping method using variable TR's can be used.

One limitation of the smoothing  $B_1$  estimation is it combines both transmit and receive  $B_1$  fields. Further improvements can include an independent acquisition for  $B_1^+$  and  $B_1^-$  measurements (20,21) and calibration of both  $B_1$  and  $M_0$  in expense of extra scan time. If the dual-acquisition SPGR methods are combined with an independent  $B_1^+$  measurement [c.f., Ref. (20)] for accuracy, then it can supersede the current proposed method in precision.

Another limitation of this study is the assumption of very short TE that might lead to an underestimation of  $M_0$  in cases where there are tissue components with short  $T_2^*$  relaxation time. In summary, the experimental results from healthy volunteers' images confirmed that the proposed method enables high-resolution quantitation of  $B_1$  and  $M_0$  maps within a clinically tolerable scan time. In comparison with existing methods (10,11,15, 22, 23), both  $B_1$  and  $M_0$  showed a good correlation within the expected range of accuracy. The intrinsic correction for the  $B_1$  inhomogeneity and stability of a single-scan approach provides a reliable method with a large and flexible range of accuracy. Major systematic errors were compensated and the SNR was optimized for human brain imaging at 3.0 T; although the described framework offers sufficient flexibility to optimize the experimental protocol for different applications or different constraints. This allows the method to be readily used for imaging applications in clinical settings.

## V. CONCLUSIONS

A non-invasive, simple, and straightforward method for quantitative measurement of MR magnetization vector has been presented, which is based on the linearization of 3D SPGR MR sequences. Quantitative magnetization vectors with an isotropic spatial resolution of  $1 \times 1 \times 1 \text{ mm}^3$  that covers a large volumetric object were achieved in less than 5

minutes. The results clearly demonstrate that fast SPGR sequences based on the variable flip angle and repetition times approaches with appropriate parameter settings can obtain a full description of the MR magnetization vector that is suitable for a variety of experimental physics clinical applications.

## VI. REFERENCES

- [1]. Carr HYSteady-state free precession in nuclear magnetic resonance *Phys Rev* 1958; 112: 1693–1701.
- [2]. Oppelt A, Graumann R, Barfuss H, Fischer H, Hartl W, Shajor WFISP — a new fast MRI sequence *Electromedica* 1986; 54: 15-8.
- [3]. Scheffler K, Lehnhardt S Principles and applications of balanced SSFP techniques *Eur Radiol* 2003; 13: 2409-18
- [4]. Leupold J, Hennig J, Scheffler K Alternating repetition time balanced steady state free precession *Magn Reson Med* 2006; 55: 557-65.
- [5]. Hargreaves BA, Vasanawala SS, Nayak KS, Hu BS, Nichimura DG Fat-suppressed steady-state free precession imaging using phase detection *Magn Reson Med* 2003; 50: 210-3.
- [6]. Absil J, Denolin V, Metens T Fat attenuation using a dual steady-state balanced-SSFP sequence with periodically variable flip angles *Magn Reson Med* 2006; 55: 343-51.
- [7]. Deoni SC, Rutt BK, Peters TM Rapid combined T1 and T2 mapping using gradient recalled acquisition in the steady state *Magn Reson Med* 2003; 49(3):515–26.
- [8]. Preibisch C, Deichmann RT1 mapping using spoiled FLASH-EPI hybrid sequences and varying flip angles *Magn Reson Med* 2009; 62(1):240–6.
- [9]. Helms G, Dathe H, Dechent P Quantitative FLASH MRI at 3 T using a rational approximation of the Ernst equation *Magn Reson Med* 2008; 59(3):667–72.

- [10]. Neeb H, Zilles K, Shah NJ A new method for fast quantitative mapping of absolute water content in vivo *Neuroimage* 2006;31(3):1156–68.
- [11]. Sabati M, Maudsley AA Fast and high-resolution quantitative mapping of tissue water content with full brain coverage for clinically-driven studies *Magn Reson Imaging* 2013;31(10):1752–59.
- [12]. Zong M1, Yan C, Lu L, Shi HB, Yu RB Feasibility of Dual Flip Angle-Based Fast 3-Dimensional T1 Mapping for Delayed Gadolinium-Enhanced Magnetic Resonance Imaging of Cartilage of the Knee: A Histologically Controlled Study *J Comput Assist Tomogr* 2016;40(3):442–6.
- [13]. Sabati M, Maudsley AA Clinically-driven fast and high-resolution mapping of T1, M0, and B1 with whole brain coverage *Proc 18th ISMRM Stockholm, Sweden; 2010* p2317.
- [14]. Volz S, Noth U, Deichmann R Correction of systematic errors in quantitative proton density mapping *Magn Reson Med* 2012;68(1):74–85.
- [15]. Neeb H, Ermer V, Stocker T, Shah NJ Fast quantitative mapping of absolute water content with full brain coverage *Neuroimage* 2008;42(3):1094–109.
- [16]. Johanson CE, Duncan 3rd JA, Klinge PM, Brinker T, Stopa EG, Silverberg GD Multiplicity of cerebrospinal fluid functions: new challenges in health and disease *Cerebrospinal Fluid Res* 2008;5:10
- [17]. Gasparovic C, Neeb H, Feis DL, Damaraju E, Chen H, Doty MJ, South DM, Mullins PG, Bockholt HJ, Shah NJ Quantitative spectroscopic imaging with in situ measurements of tissue water T1, T2, and density *Magn Reson Med* 2009;62(3):583–90.
- [18]. Volz S, Noth U, Deichmann R Correction of systematic errors in quantitative proton density mapping *Magn Reson Med* 2012;68(1):74–85.
- [19]. Cordes D, Yang Z, Zhuang X, Sreenivasan K, Mishra V, Hua LHA new algebraic method for quantitative proton density mapping using multi-channel coil data *Med Image Anal* 2017;40:154–171
- [20]. Voigt T, Nehrke K, Doessel O, Katscher UT1 corrected B1 mapping using multi-TR gradient echo sequences *Magn Reson Med* 2010;64(3):725–33.
- [21]. Yarnykh VL Actual flip-angle imaging in the pulsed steady state: a method for rapid three-dimensional mapping of the transmitted radiofrequency field *Magn Reson Med* 2007;57(1):192–200.
- [22]. Warntjes JB, Dahlqvist O, Lundberg P Novel method for rapid, simultaneous T1, T\*2, and proton density quantification *Magn Reson Med* 2007;57(3):528–37.
- [23]. Meyers SM, Kolind SH, MacKay AL Simultaneous measurement of total water content and myelin water fraction in brain at 3T using a T2 relaxation based method *Magn Reson Imaging* 2017;37(4):187–194.